MODELLING OF THE IMPACT OF MELT SURFACE DYNAMICS ON A PHOTODIODE MONITORING SIGNAL IN LASER WELDING

Paper 526

Peter Norman, Hans Engström, Alexander F.H. Kaplan

Division of Manufacturing Systems Engineering, Luleå University of Technology
SE-971 87 Luleå, Sweden

Abstract

Today merely a few monitoring systems for in-process detection of laser welding defects are commercially available. Despite a trend towards cameras, the industrially most powerful concept is still a photodiode with optical filter, measuring thermal emissions from the melt surface and from the plasma or laser beam reflections. The monitoring rule for each application is identified empirically through temporal correlations between dynamic signal changes and obtained welding defects. The mechanisms behind are widely not understood. Thus the method does not provide a systematic estimation of success for identifying a certain welding defect.

The here presented research approach studies the context between welding defects, the physical mechanisms behind, particularly the dynamics of melt pool, plasma and temperature field, and the photodiode signal. Numerical simulation results of the thermal emissions from the weld pool and keyhole dynamics and their non-linear conversion into a voltage signal are presented. An essential outcome is the sensitivity of the sensor signal to certain sub-mechanisms of the motion for judging under which conditions they can be monitored. Various results are discussed for simplified hypothetic cases as well as for observed weld pool dynamics of practical relevance.

Introduction

Laser welding is a highly complex process governed by the interaction of several optical, thermodynamic and fluidmechanic mechanisms. As the resulting quality of the weld is essential for industrial applications but sensitive to the process parameters, improved process understanding as well as in-process monitoring is desired. Welding defects like lack of fusion, lack of penetration, cold laps, undercuts, holes, pores or cracks have to be avoided.

Commercial process monitoring systems either detect thermal emissions or laser reflections from the dynamic welding process by photodiodes or by cameras. Surveys on process monitoring during laser processing are given by several authors [1-3]. The melt or plasma dynamics is often in direct or indirect context with the generation of welding defects and can therefore be suitable for their on-line detection. Photodiode detection has the advantage of delivering a robust signal as a function of time, easy to handle, but the reduction to a single voltage signal corresponds to loss of information due to its integrative nature (in terms of space, wavelength). In contrast, monitoring by a camera provides an image of the process with lot of information, but requires complex signal analysis, difficult to realise in industry in a robust, universal and reliable manner. The present study focuses on analysis of the generation of commercial [4] photodiode signals by the welding process, in particular on its mathematical prediction and analysis by correlating surface motions to the signal dynamics. The main objective of the present research is improved understanding of the context between process dynamics and signal changes in order to judge the probability for correlations.

Improved understanding of the process physics can be achieved by experimental observation of the welding process with high speed imaging. An in-house developed X-ray imaging system combined with a high speed camera was developed by Matsunawa and Katayama [5]. This set-up visualizes the keyhole and melt pool motion. With these tools it was explained how the keyhole dynamics, liquid motion in the melt pool and the plasma affect the welding result, e.g. pore formation. For the explanation of spatter or humping, high speed imaging of the melt surface can be more suitable (with spectral narrow illumination for eliminating the plasma radiation).

In addition, to understand the physics and mechanisms behind the laser welding process, mathematical modelling and simulation can be applied. Even with today's computer powers, the laser welding process has been too complex to be

fully simulated, but there are several successful results in simulating parts of the process. Amara [6] models the keyhole and melt pool movement that is affected by the flow of the metal vapour in Nd:YAG laser welding. Such dynamic keyhole simulation with melt flow and drop ejection calculation is shown in Fig. 1, explaining why the melt surface behind the keyhole has high susceptibility for drop ejection or for humping.

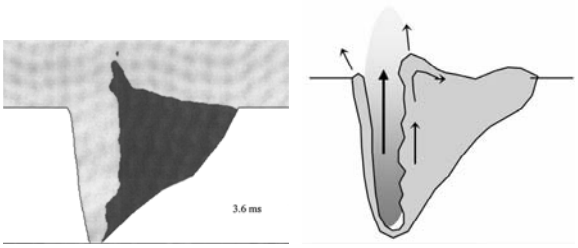

(a) (b)

Fig. 1: (a) Simulation of the keyhole and melt pool flow, (b) explaining drop ejection [6]

Other work presented by Fabbro [7,8] explains the keyhole behaviour and how the melt pool and vapour are coupled. This is done by simulating the movement of the melt pool, metal vapour plume and keyhole during Nd:YAG laser welding, supported by high speed imaging of the weld pool motions.

Jin [9] models the keyhole in 3D by imaging the keyhole during welding and from this data building the model. This model is based on welding in glass. Despite significant progress, still no complete prediction or description of the laser welding process, in particular of its context to welding defects has been achieved. Rai [10,11] models the keyhole and weld pool geometry using numerical modelling based on heat transfer models. Ye [12] shows that both Marangoni and natural convection has an impact on the weld geometry even for keyhole welding.

A model for explaining pore formation during the keyhole collapse after the end of a laser pulse [13] (for simplifying liquid metal environment) is shown in Fig. 2, explaining that recondensation of the metal vapour after pulse termination sucks the surrounding Ar-shielding gas into the keyhole that closes to a cavity during the collapse. During contraction the cavity ends in a stable spherical bubble where the surface tension pressure is in balance with the trapped Ar gas volume. During resolidification the slowly rising bubble turns to a pore.

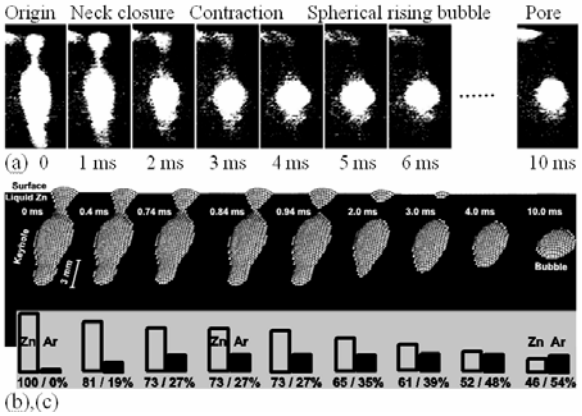

Fig. 2: Keyhole collapse towards a bubble after termination of a laser pulse: (a) time sequence of X-ray images of the keyhole (side view), (b) contraction predicted by the model, (c) calculated mixture of metal vapour (Zn) and shielding gas (Ar) in the keyhole/cavity [13].

Methodological approach

Figure 1 illustrates the basic concept [14] for improving knowledge on the context between process dynamics and a generated photodiode signal.

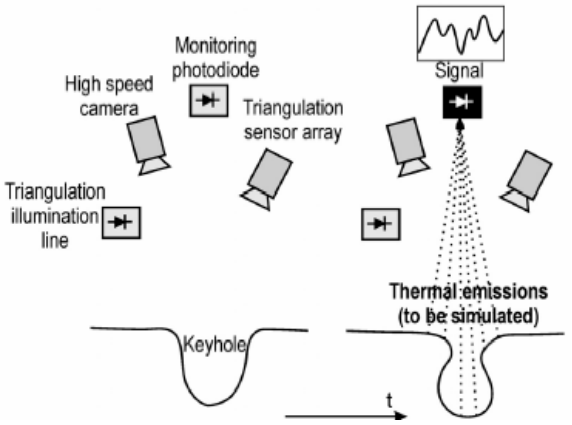

Fig. 3: Cooperative process analysis by (a) observation of the welding process with three sensors, (b) simulation of the emissions that generate a signal

The transient portion of thermal emissions from the melt and vapour (for CO_2-lasers: plasma) of a laser welding process is detected by a photodiode sensor, converting it to a time dependent voltage signal. Assuming that the melt pool emissions prevail over vapour radiation, the temperature distribution and geometry of the melt surface is responsible for the signal.

The 3D-geometry and -motion of the melt pool surface is observed qualitatively by high speed imaging (illuminated e.g. with a diode laser) and measured quantitatively by the triangulation technique where lines are projected onto the melt surface and the inclined profile is detected by a camera. This acquisition of the surface geometry data vs. time is subsequently applied as boundary condition for simulating the thermal emissions of the surface towards the photodiode sensor, eventually simulating the generated signal in order to enable analysis. This approach is cooperative in nature between experiment and simulation. From the analysis deeper knowledge on the context between surface motions (causing defects) and signal dynamics is expected, in particular categorising into major and minor physical effects and into defects with different probability of detection.

As a first step, hypothetical dynamic situations of the melt motion and their thermal emissions were modelled and studied, as will be presented in the following.

Mathematical model

Prescribing a certain dynamic situation of the weld, the emitted radiation incident on the sensor and the resulting voltage signal can be modelled, see Fig. 4.

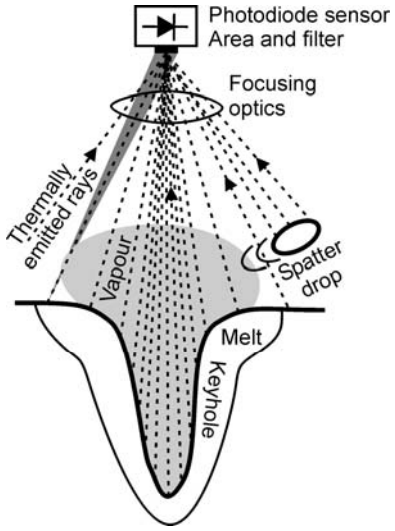

Fig. 4: Thermal emissions from the weld pool surface, incl. keyhole, vapour plume and spatter, to a photodiode sensor

Thermal radiation from the surface and from the vapour or plasma contributes to the signal, which can be considered by ray tracing of all surface elements visible by the sensor plus all vapour volume contributing. Fig. 4 illustrates that the summation of all radiation does not simply correspond to the projected surface visible by the sensor. Instead, surface domains with steeper angles (e.g. the keyhole) contribute larger according to their larger area, as was also experienced during high speed thermocamera imaging. Spatter drops shadow part of the emitting pool surface, but instead radiate by themselves. The rays travel through the metal vapour cloud and shielding gas as well as through the focusing optics. The sensor has a certain size, see Fig. 4, and is thus hit by a small cone/pyramid (of angle φ) rather than a ray of light, see Fig. 5 and Fig. 4, left, described by a view factor C_v. Surfaces have a certain angle-dependent radiation characteristics with the power density depending on the angle to the normal by $\cos(\theta)$. Moreover, radiation propagating in the cone decreases at distance r by $1/r^2$ corresponding to an expanding spherical surface area.

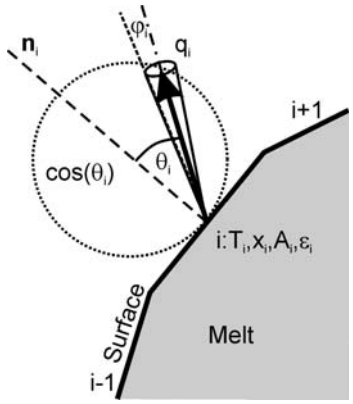

Fig. 5: Thermal radiation flux q_i from a liquid surface element *i* to the sensor

For a certain surface element i, Fig. 5 also illustrates that the power density of each ray/cone depends on the surface element area A_i, on the temperature T_i and on the emissivity ε_i. Thermal emissions are generally governed by Planck's radiation law in terms of power density per spectra λ [W/m^{-3}]:

$$dq(\lambda;T) = \frac{4\pi hc}{\lambda^5}\frac{1}{\exp\left(\frac{hc}{k_B T\lambda}\right)-1}d\lambda \qquad (1)$$

(wavelength λ, Planck's constant h, vacuum speed of light c, Boltzmann's constant k_B)

As a first step the spectral behaviour (emissivity, Planck's law, sensor characteristics) will not be taken

into account, thus the spectrally integrated version of Planck's law, the Stefan-Boltzmann law will be applied, with the power density proportional to the fourth power of temperature:

$$q_{tot} = \varepsilon\sigma_{SB}\left(T^4 - T_a^4\right) \qquad (2)$$

(Stefan-Boltzmann constant σ_{SB} = 5,6703·10^{-8} W/m^{2}K^4, ambient temperature T_a)

A single surface element contributes to the power irradiating the sensor at inclination angle θ by:

$$P_{si} = A_i \cos^2\left(\theta_i\right) C_{vi}\varepsilon_i\sigma_{SB}\left(T_i^4 - T_a^4\right) \qquad (3)$$

Note the squared cos(θ)-dependence, originating both from the emission characteristics and from the projection. As in the present study, the sensor usually is at a distance (R_s = 200 mm) far away and its area (A_s = 25 mm^2) appears small (same for the surface element). Moreover, close to normal incidence ($\theta \approx 0$), the view factor can be simplified to:

$$C_v = \frac{A_s}{2R_s^2\pi} \qquad (4)$$

here resulting in C_v = 9,95·10^{-5}.

The above described the radiation contribution by a single surface element. The power incident on the sensor, governing the signal, results from integration over all surface elements (area A_{tot}) according to Fig. 4.

$$P_s(t) = \frac{1}{A_{tot}} \int_{x,y} P_i(t)\,dx\,dy \qquad (5)$$

The signal, i.e. the sensor voltage as a function of time results from this incident power, when taking into account by integration the spectral weighting by the spectral sensor transition function (including its absorption) f_s and possible additional spectral filters f_f arranged (e.g. UV-low pass for plasma detection):

$$U_s(t) \propto \int_{\lambda 1}^{\lambda 2} P_s(t;\lambda) f_s(\lambda) f_f(\lambda)\,d\lambda \qquad (6)$$

In the present study only $P_s(t)$ will be calculated. Radiation from the vapour (rather than plasma, as Nd:YAG-lasers are studied here) is neglected in first order.

Essential for process monitoring is that this radiation towards the sensor is governed by melt surface motion and by temperature changes, which sometimes correlates with welding defect mechanisms. Basically any dynamic situation can be studied with the here presented model. The investigations start with very simple hypothetical oscillation cases, to be step by step developed towards more sophisticated consideration of effects (geometry, wavelength, vapour, combination). Eventually the motions and temperature fields observed from high speed imaging experiments will be the boundary condition for the model, in order to explain them in context with observed sensor signals.

The simplest case studied is based on a radially symmetric solution of the heat conduction equation for a point source of heat (absorbed laser power), having constant average power P_0, superimposed by an oscillatory power with amplitude P_1 and frequency f_p or $\omega_P = 2\pi f_P$

$$P(t) = P_0 + P_1 \sin\left(\omega_P t\right) \qquad (7)$$

resulting in the temperature field [15]

$$T(r;t) = T_a + \frac{1}{4\pi K r}\left[P_0 + P_1 \sin\left(\omega_P t + kr\right)\right]\exp\left(-kr\right) \qquad (8)$$

with

$$k = \sqrt{\frac{\omega_P}{2\kappa}} \qquad (9)$$

where K is the thermal conductivity and κ is the thermal diffusivity. The model is illustrated in Fig. 6.

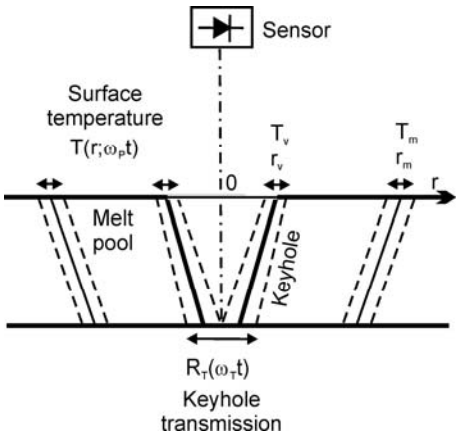

Fig. 6: Mathematical model of laser welding by a simplified oscillating temperature field and keyhole bottom opening

No welding speed is considered, simplifying all to a rotationally symmetrical problem, like spot welding or low welding speed situations.

From this temperature field, Eq.(8), by numerical integration the power incident on the sensor can be calculated as a function of time via Eq.(3),(5).

As a next step, a second mechanism can be superimposed, thus competing with the first mechanism, resulting in a more complex signal. From the first model an (oscillating) evaporation isotherm results, with a minimum radius $R_{kh,min}$. It is assumed that the temperature remains the boiling temperature inside, the angle contribution of the inclined wall is neglected here for simplicity. As the second mechanism, it was assumed that this keyhole is open at the bottom (welding through) and that the transmission opening radius $R_T < R_{kh,min}$ oscillates by

$$R_T(t) = R_{T1}\left(1 + \sin\left(\omega_T t + \varphi_T\right)\right)/2 \qquad (10)$$

(frequency $\omega_T = 2\pi f_T$, phase shift φ_T), see Fig. 6, thus it just closes and then opens again to a maximum radius in a harmonic manner. The open central domain transmits laser radiation but does not emit to the sensor. Just the remaining part of the vapour zone is assumed to contribute like a flat surface, for sake of simplicity. Again, this portion leads to a certain power (reduction) on the sensor. Thus actually two power contributions (or signals) are superimposed, and their visibility in the signal is based on competition between them and on nonlinear physical mechanisms.

A third mechanism could e.g. be the travelling of a drop, see Fig. 4, that also contributes with its radiation (and shadowing) to the sensor signal, including the drop's inclined surface and its temperature.

Results and discussion

Numerical results for the above two sub-models were calculated for low C-steel (emissivity of $\varepsilon = 0.9$ assumed). Three cases were studied according to Tab. 1 and Eqs.(7),(10).

Table 1: Parameters of the three cases studied

Case		A	B	C
P_0	[W]	300	300	300
P_1	[W]	30	150	150
$2R_{T1}$	[µm]	170	170	85
f_P	[Hz]	100	100	100
f_T	[Hz]	700	700	700

Sub-model 1 has a power P_0 = 300 W, plus P_1 = 30 W or P_1 = 150 W, respectively, for two cases studied, with a frequency of f_P = 100 Hz.

Figure 7 shows for Case B the surface temperature field as a function of the radius for three time steps (0, 2.5, 7.5 ms, for the 10 ms sinus-period). The strong power oscillation P_1 results in a damped oscillation of the temperature field (contributing to the sensor power P_s by fourth power of T), and in corresponding oscillations of the melt pool and keyhole size, including phase shifts.

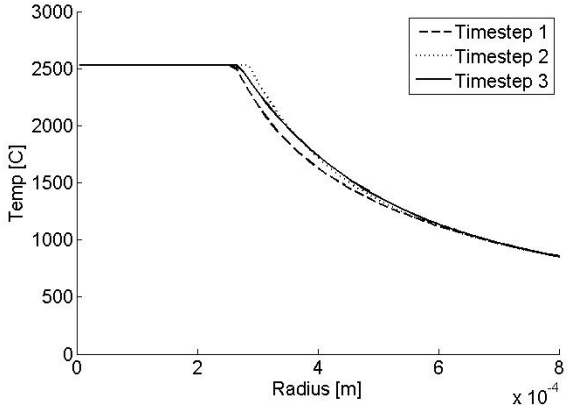

(a)

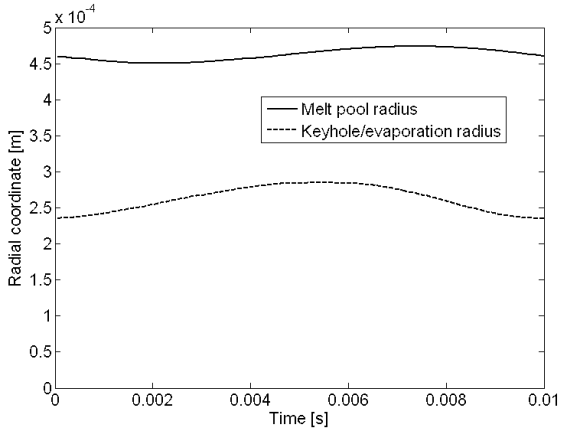

(b)

Fig. 7: Case B: (a) oscillating temperature field at the melt pool surface for the time steps t = 0, 2.5, 7.5 ms; (b) surface melt and evaporation radius vs. time

The oscillations led to a minimum evaporation/keyhole radius of $R_{kh,min}$ = 230 µm. A smaller radius was chosen for the keyhole bottom opening: R_{T1} = 85 mm for Case A,B and R_{T1} = 42,5 µm for Case C. The frequency for the keyhole transmission oscillations was assumed seven times higher, thus f_T = 700 Hz.

It should be emphasized that the here assumed values, particularly the frequencies, are purely hypothetically. Later, high speed imaging will be applied for identifying real values that could differ strongly. However, for the present fundamental study, this is not of importance. Instead the possibilities for analysis, particularly for sensitivity of different contributions and their mechanisms will be studied. For the integration, a radial discretisation of 10 μm turned out sufficient. A time discretisation of 5 μs was chosen, but does not affect the results, as the semi-analytical calculation scheme is explicit.

Fig. 8 shows the calculated sensor signal for Case B. The envelope is here governed by the slower power-driven temperature oscillation, while the higher frequency component results from the keyhole opening oscillations. Even for this strongly simplified model already a rather complex nonlinear signal results. The signal will become more complex, imagining the many sub-mechanisms and irregular motions normally involved.

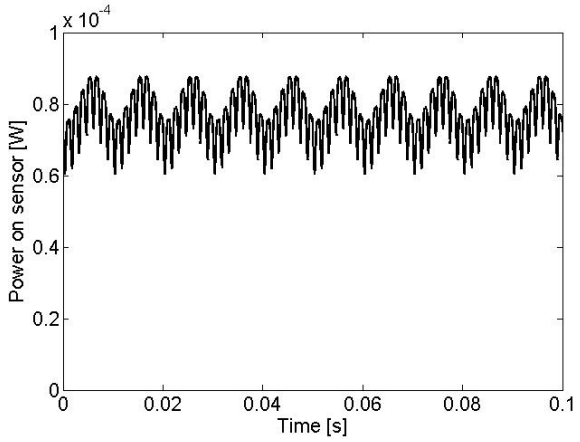

Fig. 8: Calculated emission power $P_s(t)$ incident on the sensor (signal) as a function of time (case B)

For the three cases studied, one main cycle of the purely temperature field governed signal (dotted) as well as of the combined signal (with keyhole opening) is plotted in Fig. 9(a)-(c) for the three Cases A-C, respectively.

As can be seen for Case A, the temperature field governed signal with the lower frequency is the envelope of the keyhole opening oscillation. For Case A the contribution from the keyhole opening is dominant, Case B is composed of about equal contributions, for Case C the temperature field is dominant.

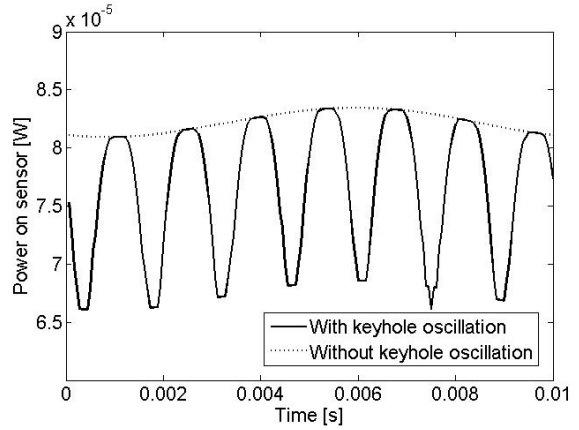

(a)

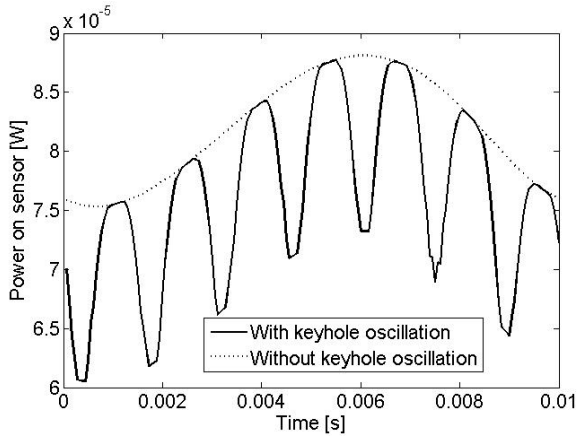

(b)

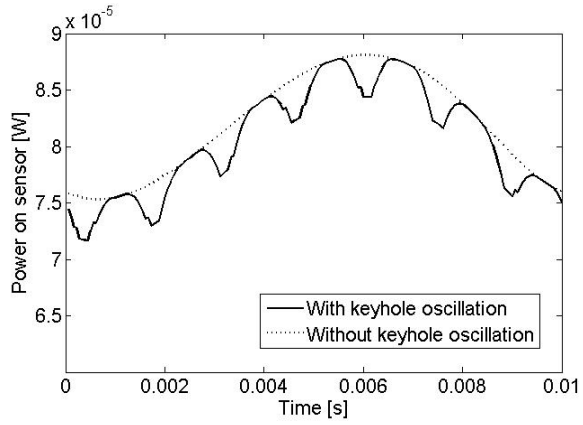

(c)

Fig. 9: Emission power $P_s(t)$ incident on the sensor vs. time: (a) Case A: P_1 = 30 W, $2R_{T1}$ = 170 μm, (b) Case B: P_1 = 150 W, $2R_{T1}$ = 170 μm, (c) Case C: P_1 = 150 W, $2R_{T1}$ = 85 μm

For deeper analysis of the two non-linear contributions, the percentage of maximum (not average) contribution to the power incident on the

sensor (signal) as a function of the radial coordinate is plotted in Fig. 10 for the three cases. It can be distinguished between the keyhole opening area, where the radius contributes in a quadratic manner (for constant temperature), the keyhole wall region (not contributing to oscillations in this model, thus plateau) and the surface radiation from the melt and solid, that still contributes with the radius squared. However, the temperature then drops exponentially, contributing by the fourth power, thus the larger area becomes less dominant than the decreasing temperature.

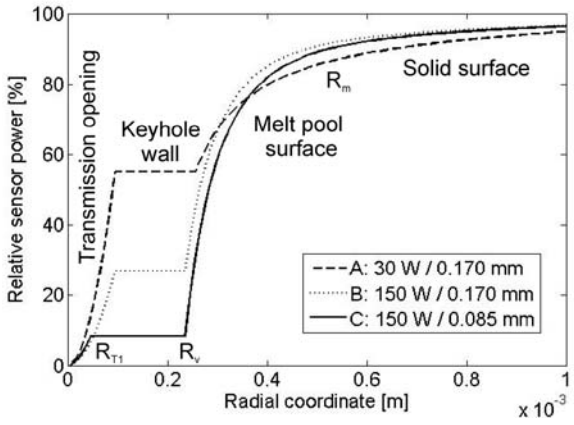

Fig. 10: Relative contribution of different spatial domains to the oscillating part of the power/sensor signal $P_s(t)$ for the three cases (P_1, $2R_{T1}$)

Note that the mean value of the oscillations does not contribute to signal dynamics and is not useful for monitoring, thus only the (maximum) oscillating value is shown here. Consequently, for Case A ,with low power peak but wide keyhole opening, the keyhole contribution becomes essential (57 %). In contrast, for Case C the little keyhole transmission opening is weak (8 %) against the strong power and temperature oscillation, however, mainly in the hot region close to the keyhole. Case B is in between (27 %).

With such kind of modelling and analysis, two competing mechanisms contributing to a signal can be compared to each other. Step by step more sophisticated modelling will lead to deeper analysis and eventually experimental observations are aimed to feed the simulation as real input, in order to analyse the real defect mechanisms taking place.

Conclusions

- The context between thermal welding process emissions and a resulting photodiode signal is not yet understood
- Modelling of the context between melt surface motions and the sensor signal permit detailed analysis of the dominant mechanisms
- Even very simple hypothetical cases already generate complex signals
- Even very small oscillations can become dominant in the signal
- For power and thus temperature field oscillations of the weld, competing with keyhole opening oscillations, each mechanism can become dominant in the signal - depending on the parameters
- The fourth power of the temperature rapidly weakens the contributions of regions at lower temperature, despite larger area
- The model has the potential for clear, detailed analysis of the physical mechanisms involved
- The model has the potential for analysis of more sophisticated situations, in particular for motions observed from high speed imaging

Acknowledgements

The authors are grateful to VINNOVA – The Swedish Innovation Agency (project DATLAS, no. 27744-2, project HYBRIGHT, no. 27382-2, and project LOST, no. 2006-00563), to the Kempe Foundation and to the Research Council of Norrbotten for funding the research.

References

[1] Norman, P., Engström, H. & Kaplan A. F. H. (2007) State-of-the-Art of monitoring and imaging of laser welding defects, NOLAMP 11: The 11th Nordic Conference in Laser Processing of Materials, Lappeenranta, Finland, 2007, Aug. 20-22

[2] Kaierle, S., Abels, P. & Kratzsch, C. (2005) Proc. LIM, Munich, June 2005, Ed: E. Beyer, WLT, 101-105.

[3] Shao, J. & Yan, Y. (2005) Review of techniques for on-line monitoring and inspection of laser welding, Journal of Physics: Conference Series 15, 101-107.

[4] Kogel-Hollacher, M., Nicolay, T., Kattwinkel, A., Muller, M.G. & Muller, J. (2004) On-line process monitoring in laser material processing-techniques for the industrial environment, Proc. PICALO 2004, Melbourne, April 2004, LMP-SC, 1-4.

[5] Matsunawa, A. & Katayama, S. (2002) Understanding physical mechanisms in laser welding for construction of mathematical models, Welding in the World, 46, 27-38.

[6] Amara E. H., Fabbro, R. & Hamadi, F. (2006) Modeling of the melted bath movement induced by the vapour flow in deep penetration laser welding, Journal of Laser Applications, 18, 2-11.

[7] Fabbro, R., Slimani, S., Doudet, I., Coste, F. & Briand, F. (2006) Experimental study of the dynamical coupling between the induced vapour plume and the melt pool for Nd:YAG CW laser welding, J. Phys. D: Applied Physics, 39, 394-400.

[8] Fabbro, R., Slimani, S., Coste, F. & Briand, F. (2005) Study of keyhole behaviour for full penetration Nd:YAG CW laser welding, Journal of Physics D: Applied Physics, 38, 1881-1887.

[9] Jin, X., Berger, P. & Graf, T. (2006) Multiple reflections and Fresnel absorption in an actual 3D keyhole during deep penetration laser welding, Journal of Physics D: Applied Physics, 39, 4703-4712.

[10] Rai, R. & DebRoy, T. (2006) Tailoring weld geometry during keyhole mode laser welding using a genetic algorithm and a heat transfer model Journal of Physics D: Applied Physics, 39, 1257-1266.

[11] Rai, R., Roy, G.G. & DebRoy, T. (2006) A computationally efficient model of convective heat transfer and solidification characteristics during keyhole mode laser welding, Journal of Applied Physics, 101, 54909-1-11

[12] Xiao-Hu, Y. & Xi, C. (2002) Three-dimensional modeling of heat transfer and fluid flow in laser full-penetration welding, Journal of Physics D: Applied Physics, 35, 1049-1056

[13] Kaplan A. F. H., Mizutani, M., Katayama, S. & Matsunawa, A. (2002) Unbounded keyhole collapse and bubble formation during pulsed laser interaction with liquid zinc, Journal of Physics D: Applied Physics, 35, 1218-1228

[14] Engström, H., Norman, P. & Kaplan A. F. H, (2007) DATLAS: A new approach for monitoring the laser welding process, NOLAMP 11: The 11th Nordic Conference in Laser Processing of Materials, Lappeenranta, Finland, 2007, Aug. 20-22

[15] Carslaw, H.S. & Jaeger, J. C. (1959) Conduction of heat in solids, Oxford Clarendon, 263.

Meet the Authors

Peter Norman was born in Luleå in the north of Sweden in 1974. He studied mechanical engineering at Luleå University of Technology, got a Bachelors degree in 1997 and graduated at the Master level in 2002. He worked at a steel mill as researcher for two years, and after that returned to the university as PhD-student, receiving the Technical Licentiate degree on process monitoring of milling in 2006.

Hans Engström was born in Luleå, Sweden in 1951. He carries out research in different areas of laser materials processing at Luleå TU for more than 25 years, e.g. for his Licentiate thesis on laser cladding. Moreover, he is deputy head of division and he teaches LEAN manufacturing to Swedish industry.

Alexander Kaplan was born in Vienna, Austria in 1967, employed as researcher at Vienna TU from 1989 until 2000, receiving a PhD-degree in 1994. After a post-doc year at Osaka University, Japan, from 2002 on he has been appointed as professor and head of division on manufacturing at Luleå University of Technology, Sweden. His research focus comprises laser materials processing, in particular process modelling, laser welding and hybrid welding.